

Analysis of the mechanical deformation arising from investment casting of directionally solidified nickel-based superalloys

C. Panwisawas*¹, J.-C. Gebelin² and R. C. Reed³

To provide insight into the factors causing recrystallisation of nickel-based single crystal superalloys, analysis of the thermal–mechanical deformation caused by investment casting of these components is presented. Three-dimensional thermal–mechanical finite element analysis is first used to demonstrate that the reaction of the casting and mould—at least in the aerofoil section—can be approximated as one-dimensional. One-dimensional models are then built based upon static equilibrium for plasticity on the microscale caused by differential thermal contraction of metal, mould and core, using temperature dependent material properties. The models take various forms to study the mechanical response under different situations relevant to practical applications. The results indicate that the plastic strain causing recrystallisation is likely to be induced during cooling at temperatures above 1000°C. The relative importance of thicker and stiffer ceramic shells is studied. Our analysis indicates that it is important to account for creep deformation for such applications.

Keywords: Mechanical deformation, Solidification, Investment casting, Superalloys

Introduction

Turbine blades used for jet engine applications are investment cast from nickel based superalloys, often in single crystal form. However, recrystallisation can occur—with associated grain boundaries thus introduced—during the subsequent heat treatment steps needed to remove the interdendritic microsegregation inherited from solidification processing.^{1–4} This is an issue particularly for modern aerofoils, which have intricate cooling passages, of the type needed to restrict metal temperatures to reasonable levels.⁵

Despite its importance for practical applications, very little is known about the factors causing recrystallisation in these alloys.^{6,7} Answers to some critical questions are needed. For instance, at what temperature is the plastic strain causing recrystallisation induced in the casting?^{8,9} What is the influence of the relative cross-sections of mould and metal? Is there any influence of cooling rate?¹⁰ What are the relative importance of the various material properties needed to describe the process?^{11,12} Answers to these fundamental questions would aid in the design of more efficient foundry practice and better

processing-friendly blade designs and provide concomitant benefits in terms of fuel economy and performance. That modelling can be used to analyse this process has been proven,¹³ with a thermal model of the solidification of a single crystal investment casting being coupled with a microstructural analysis of the competitive grain growth process.

The work reported in the present paper was carried out with the above in mind. Numerical analysis is presented to identify the factors causing casting-induced plasticity¹⁴ and thus recrystallisation in these materials. The relative importance of the different thermal–physical and mechanical properties are accounted for. We concentrate particularly on a simplified one-dimensional (1D) analysis having shown this to be largely valid, although it should be noted that the physical descriptions employed are quite generic and therefore well suited for more sophisticated analyses in two- or even three-dimensional, which might become possible in the future.¹⁵

Background: mechanical deformation during investment casting

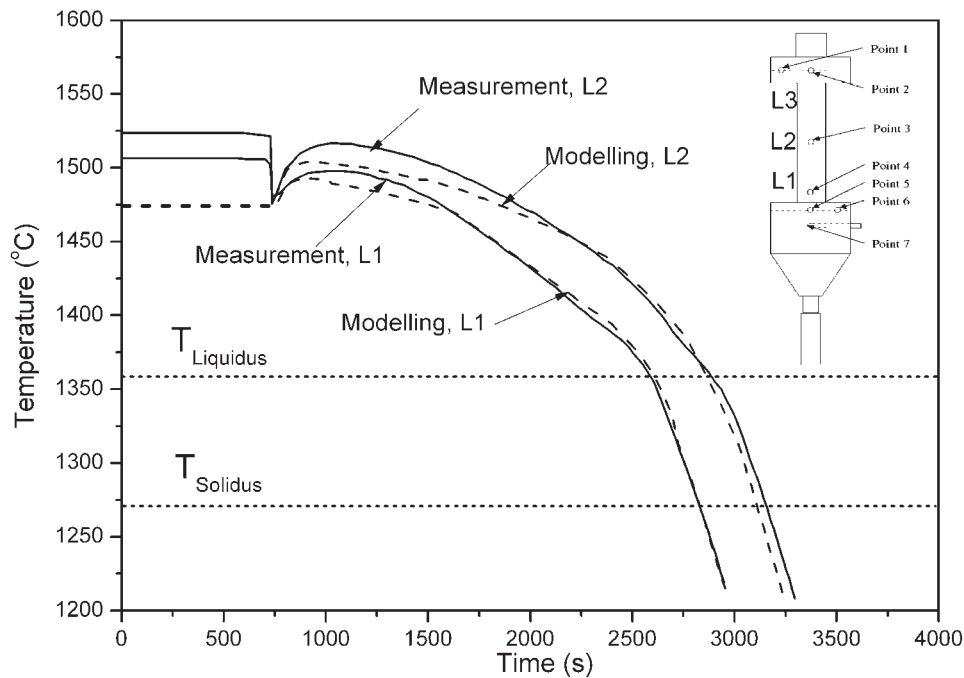
In order to place the present work in context, the results of a thermal–mechanical analysis of the casting of a representative turbine blade geometry are considered first. It is not the purpose of the present paper to consider the methods used in great detail; instead, the results are used to inspire the further more detailed analysis that is presented in the rest of the paper. For simplicity, a solid casting is analysed of representative

¹Partnership for Research in the Simulation of Manufacturing and Materials (PRISM²), Department of Metallurgy and Materials, University of Birmingham, Edgbaston, Birmingham B15 2TT, UK

²Doncasters Group Ltd, Doncasters Precision Castings - Deritend Ten Acres, Droitwich, Worcester WR9 9BP, UK

³Department of Engineering Science, University of Oxford, Parks Road, Oxford OX1 3PJ, UK

*Corresponding author, email CXP864@bham.ac.uk



1 Temperature measurement in VeriCAST model reported by Newell¹⁷

dimensions, without the cooling passages that are usually present. The shroud and platform regions are typical of those seen on a real component. The thermal analysis of this problem and geometry has been presented in detail by Dai *et al.*;¹⁶ however, the mechanical behaviour has not been investigated as yet.

The geometry has been christened the VeriCAST casting. It processed a withdrawal rate from the furnace of $6.36 \times 10^{-5} \text{ m s}^{-1}$; the cooling rate is estimated to be $\sim 0.83^\circ\text{C s}^{-1}$ at a temperature of 1300°C . The casting is made from the CMSX-4 superalloy using an alumina based shell material; these are assumed to be plastically deformed and elastically deformed respectively; temperature dependent materials along solidification direction $\langle 001 \rangle$ are employed under the assumption of elastic isotropy. Following Newell,¹⁷ validation of the thermal model has been performed using an industrial scale investment casting facility at the University of Birmingham. It can be seen that the thermal model recovers accurately the thermocouple readings (Fig. 1). Our analysis indicates that the effective stress in the turbine aerofoil cross-section does not vary strongly within the aerofoil, provided that one is far enough away from the platform and shroud regions (Fig. 2). Figure 3 illustrates how the stress generated in the casting direction varies with temperature, at the middle of the aerofoil cross-section at midheight. The stress component is largest in the withdrawal direction and does not vary significantly across the section. This one can be seen via the definition of the effective stress (the von Mises stress) defined by

$$\sigma_{\text{eff}} = \left\{ \frac{1}{2} [(\sigma_1 - \sigma_2)^2 + (\sigma_2 - \sigma_3)^2 + (\sigma_3 - \sigma_1)^2] \right\}^{1/2} \quad (1)$$

Figure 3 essentially shows that

$$\sigma_{\text{eff}} \approx \sigma_1 \quad (2)$$

The results confirm that the stress component σ_1 in the withdrawal direction is largest with the other two components $\sigma_2 \approx \sigma_3 = 0$. Moreover, Fig. 4 confirms that

that the stress builds up at the middle position at L2 before the top position at L3 becomes totally solid.

These results indicate that it is possible to simplify the mechanical response of the system to be 1D, at least to a first approximation. In view of the many uncertainties concerning the materials data and the most appropriate constitutive equation to employ, there is value in assuming this to be the case and determining the response of the system that then occurs. This was the rationale for the work reported in the present paper.

Preliminaries

Based upon the theory of 1D linear isotropic thermal elasticity, the stress and strain behaviour of a superalloy in the solidification direction can be expressed by

$$\sigma^{\text{el}} = E \varepsilon^{\text{el}} \quad (3)$$

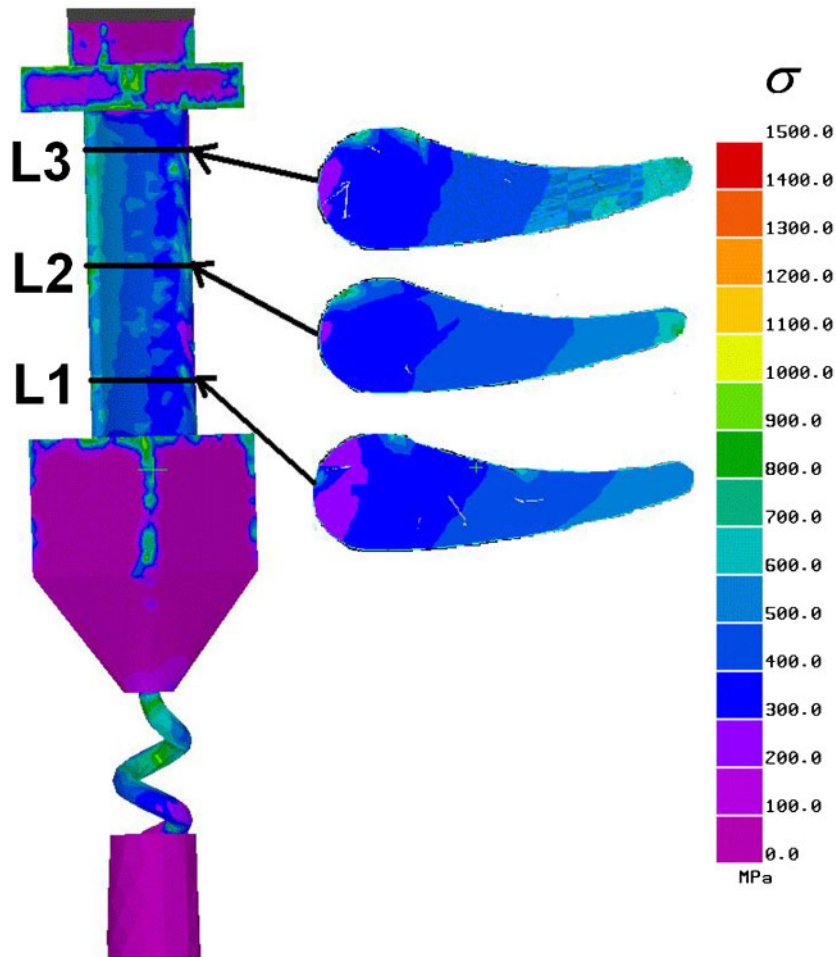
where σ^{el} , E and ε^{el} are the stress, Young's modulus and elastic strain respectively. The first assumption that can be introduced is to treat the superalloy and shell as a closed system, so that no external force is applied; consequently, the thermal contraction strain is then distributed between the elastic, plastic (time independent plastic deformation) and creep (time dependent plastic deformation) strains that are generated. The sum of strains is zero, consistent with

$$\sum \varepsilon = \varepsilon^{\text{el}} + \varepsilon^{\text{pl}} + \varepsilon^{\text{cr}} + \varepsilon^{\text{th}} = 0 \quad (4)$$

where ε^{pl} , ε^{cr} and ε^{th} are the plastic, creep and thermal contraction strains respectively. An isotropic hardening criterion can be used to describe the variation of the stress σ to the yield stress σ_y the ultimate yield stress σ_∞ and hardening exponent H according to

$$\sigma = \sigma_\infty + (\sigma_y - \sigma_\infty) \exp(-H \varepsilon^{\text{pl}}) \quad (5)$$

Throughout the calculations that follow, we take $H=0.3$. For the time dependent plastic deformation,



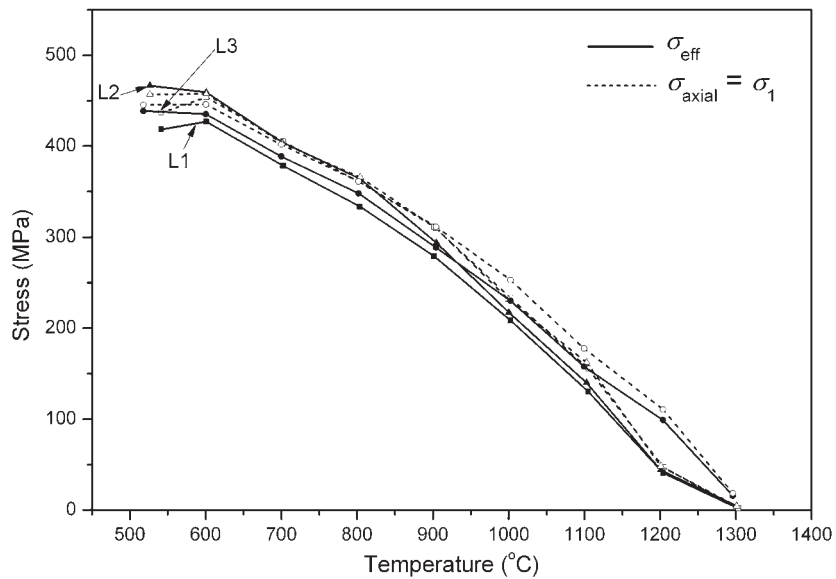
2 Effective stress results at three cross-sections of VeriCAST testpiece

we can define the creep rate from Norton’s law consistent with

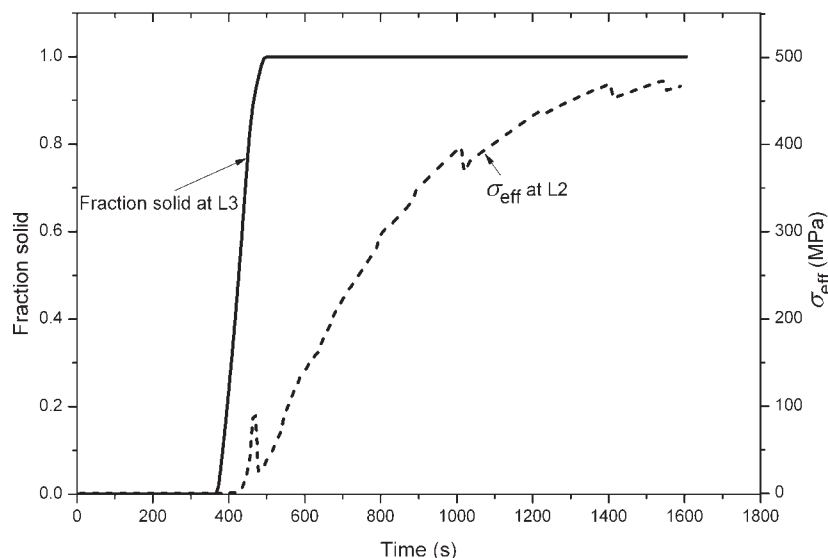
$$\dot{\epsilon}^{cr} = \frac{1}{\eta} \exp\left\{-\frac{Q}{RT}\right\} \sigma^n \tag{6}$$

where $\dot{\epsilon}^{cr} \equiv d\epsilon^{cr}/dt$, $\eta = 2.2 \times 10^{-6} \text{ s}^{-1}$ is the viscosity parameter assumed to be constant, Q is the activation

energy that is 870 kJ mol^{-1} , R is the gas constant, T is temperature and n is the stress exponent that is taken to be 10. These values should be regarded as best estimates, in the absence of the better measurements that are made later in the thesis. Where not explicitly stated otherwise, the creep strain ϵ^{cr} has been determined by integration over a temperature interval consistent with



3 Stress as function of temperature generated within VeriCAST model



4 Variation of fraction solid at location L3 and effective stress at location L2 during solidification

$$\varepsilon^{\text{cr}} = \int_{t_i}^{t_f} \dot{\varepsilon}^{\text{cr}} dt \quad (7)$$

where t_i and t_f are the initial and final times respectively. As for the thermal contraction strain ε^{th} , it is proportional to the temperature via the thermal expansion coefficient α so that

$$\varepsilon^{\text{th}} = \alpha \Delta T = \alpha(T - T_{\text{ref}}) \quad (8)$$

where T_{ref} is a reference temperature. By making use of the equations (4)–(7), equation (3) becomes

$$\sigma^{\text{el}} = E(-\varepsilon^{\text{pl}} - \varepsilon^{\text{cr}} - \varepsilon^{\text{th}}) \quad (9)$$

The stress and strain build-up within a superalloy can be calculated via the above set of equations.

Description of analysis methods

The 1D contraction of a bar of the CMSX-4 superalloy within a ceramic mould is modelled. A constraint is assumed, whereby the superalloy and shell adhere together during solidification and subsequent cooling to room temperature. The cooling rate used for the calculation is taken to be $50^\circ\text{C min}^{-1}$ ($0.83^\circ\text{C s}^{-1}$), which is representative of the investment casting process employed. Consistent with the equilibrium condition, any forces other than those arising from shrinkage are neglected. Two distinct situations are considered: the shell being completely rigid and the shell being capable of deforming elastically so that some elastic accommodation is possible.

Treatment of superalloy

For the superalloy, three distinct behaviours are considered.

Linear elastic model: no plasticity

For this case, consider equation (4): only two strains, elastic and thermal, are considered. The others are set to zero. The elastic strain in this scheme is derived directly from the thermal strain. The stress can then be obtained directly from the elastic strain and Young's modulus.

Elasto-plastic model

The above can be modified to account for the plastic strain as follows. Ignoring any time dependent creep deformation, three strains must be accounted for, namely, thermal, elastic and plastic. The thermal strain must be partitioned into elastic and plastic components. Note that when the isotropic hardening criterion of equation (5) is employed, the calculated stress will be different from that determined from the linear elastic model.

Elasto-visco-plastic model

The elasto-visco-plastic model model is likely to be the most rigorous treatment for the behaviour of the superalloy. This is because the elastic, plastic and creep strains are taken into account and decoupled. The decoupling of inelastic strains is assumed to be the sum of them and independent of each other.

Treatment of ceramic shell and core

Ceramic shell

When the elastic deformation of the shell is taken into account, it is helpful to define the ratio of cross-sectional areas S_f^s according to $S_f^s = S_{\text{alloy}}/S_{\text{shell}}$, where S_{alloy} and S_{shell} are the cross-sections of alloy and shell respectively. Consistent with the equilibrium of stress, one then has

$$S_f^s \sigma_{\text{alloy}}^{\text{el}} + \sigma_{\text{shell}}^{\text{el}} = 0 \quad (10)$$

The assumption made further is that the strain in the superalloy is equal to that in the shell

$$\varepsilon_{\text{alloy}}^{\text{el}} + \varepsilon_{\text{alloy}}^{\text{pl}} + \varepsilon_{\text{alloy}}^{\text{cr}} + \varepsilon_{\text{alloy}}^{\text{th}} - \varepsilon_{\text{shell}}^{\text{el}} - \varepsilon_{\text{shell}}^{\text{th}} = 0 \quad (11)$$

Two different shells have been studied in the present work.

Ceramic core

When the elastic deformation of a ceramic core is to be taken into account, one can in a similar way define $S_f^c = S_{\text{alloy}}/S_{\text{core}}$ so that

$$S_f^c \sigma_{\text{alloy}}^{\text{el}} + \sigma_{\text{core}}^{\text{el}} = 0 \quad (12)$$

where S_{alloy} and S_{core} are areas of the superalloy and ceramic core on a given cross-sectional plane. The

assumption made further is that the strain coming from the superalloy is equal to that from the core

$$\varepsilon_{\text{alloy}}^{\text{el}} + \varepsilon_{\text{alloy}}^{\text{pl}} + \varepsilon_{\text{alloy}}^{\text{cr}} + \varepsilon_{\text{alloy}}^{\text{th}} - \varepsilon_{\text{core}}^{\text{el}} - \varepsilon_{\text{core}}^{\text{th}} = 0 \quad (13)$$

Plasticity approximation

The plasticity within the superalloy can be calculated by making use of equation (5). By assuming that the plastic strain accumulated in the superalloy is of order 10^{-3} or less, the exponential term in equation (5) can be approximated using Taylor's series¹⁸ so that

$$\exp(x) = \sum_{n=0}^N \frac{1}{n!} x^n \quad (14)$$

In all calculations, only the first order term is kept, i.e. $N = 1$. The plastic strain can then be estimated for three cases.

Superalloy sits within perfectly rigid shell

When the elasto-visco-plastic model model is active, the plastic strain is expressed by

$$\varepsilon_{\text{alloy}}^{\text{pl}} = \frac{\sigma_y + E\varepsilon_{\text{alloy}}^{\text{th}} + E\varepsilon_{\text{alloy}}^{\text{cr}}}{H(\sigma_y - \sigma_{\infty}) - E} \quad (15)$$

In the limiting case that the elasto-plastic model is used, $\varepsilon_{\text{alloy}}^{\text{cr}}$ is set to zero in the above.

Superalloy sits in elastic shell

When making use of equations (10) and (11), a dimensionless parameter is defined according to

$$\kappa \equiv S_f^s \frac{\varepsilon_{\text{alloy}}}{\varepsilon_{\text{shell}}} \quad (16)$$

where E_{alloy} and E_{shell} are the Young's moduli of the superalloy and shell respectively. The plastic strain can now be written

$$\varepsilon_{\text{alloy}}^{\text{pl}} = \frac{\sigma_y + [\varepsilon_{\text{alloy}}/(1 + \kappa)] (\varepsilon_{\text{shell}}^{\text{th}} - \varepsilon_{\text{alloy}}^{\text{th}} - \varepsilon_{\text{alloy}}^{\text{cr}})}{H(\sigma_y - \sigma_{\infty}) - [\varepsilon_{\text{alloy}}/(1 + \kappa)]} \quad (17)$$

Once again, when the elasto-plastic model is applied, the term $\varepsilon_{\text{alloy}}^{\text{cr}}$ is set to zero.

Superalloy surrounds elastic ceramic core

In this case, the superalloy contains a ceramic core that resists its contraction. Here, it is useful to define a dimensionless parameter λ according to

$$\lambda \equiv S_f^c \frac{\varepsilon_{\text{alloy}}}{\varepsilon_{\text{core}}} \quad (18)$$

where E_{core} is the Young's modulus of the ceramic core. Taking advantage of equations (12) and (13), the plastic strain in the superalloy according to elasto-visco-plastic model model is given by

$$\varepsilon_{\text{alloy}}^{\text{pl}} = \frac{\sigma_y + [\varepsilon_{\text{alloy}}/(1 + \lambda)] (\varepsilon_{\text{shell}}^{\text{th}} - \varepsilon_{\text{alloy}}^{\text{th}} - \varepsilon_{\text{alloy}}^{\text{cr}})}{H(\sigma_y - \sigma_{\infty}) - [\varepsilon_{\text{alloy}}/(1 + \lambda)]} \quad (19)$$

If $\varepsilon_{\text{alloy}}^{\text{cr}}$ is zero, one defaults to the limiting case of the elasto-plastic model.

Stress relaxation

When the elasto-visco-plastic model model is used, creep will be taken into account. Relying on the isotropic

linear thermal elasticity used above, equation (4) is differentiated with time, so that

$$\frac{d\varepsilon^{\text{el}}}{dt} + \frac{d\varepsilon^{\text{pl}}}{dt} + \frac{d\varepsilon^{\text{cr}}}{dt} + \frac{d\varepsilon^{\text{th}}}{dt} = 0 \quad (20)$$

Simplifications to it are possible. For a given temperature, the thermal strain is constant and the plastic strain is time independent; consequently, using equation (3), one has¹⁹

$$\frac{d\varepsilon^{\text{cr}}}{dt} = -\frac{1}{E} \frac{d\sigma^{\text{el}}}{dt} \quad (21)$$

Substituting equation (6) into equation (20), a first order ordinary differential equation for the stress is arrived at

$$\frac{d\sigma^{\text{el}}}{dt} + \frac{E}{\eta} \exp\left\{-\frac{Q}{RT}\right\} (\sigma^{\text{el}})^n = 0 \quad (22)$$

This can be integrated at constant temperature to yield

$$\sigma^{\text{el}}(t) = \left[\sigma_0 - (1-n) \frac{E}{\eta} \exp\left(-\frac{Q}{RT}\right) t \right]^{1/(1-n)} \quad (23)$$

where σ_0 is the applied stress.

Calculation methods and materials data

The numerical calculations have been conducted mainly using purpose built codes within the Matlab software. Some limited calculations have been carried out via the finite element method (FEM) using the Procast software. Regardless of the calculation procedures employed, temperature dependent material properties are needed. For the CMSX-4 superalloy, mechanical data corresponding to the $\langle 001 \rangle$ direction have been taken from the literature: Young's modulus,²⁰ thermal contraction coefficient,²¹ yield strength²² and ultimate yield strength.²³ Note that some interpolation and extrapolation have been necessary to generate materials data up to 1300°C, close to solidus temperature of the superalloy. Table 1 summarises the materials data used in the present work, which are referred to as shell 1 and shell 2. The first is a Al_2O_3 based material and the second is a SiO_2 based one. Values of Young's moduli were taken from Nair and Jakus²⁴ and Pabst *et al.*,²⁵ and thermal expansion coefficients from Green²⁶ were used. Further data that were considered to be representative of a ceramic core were taken from Refs. 24–26. The assumed material data for the ceramic materials are summarised in Table 2.

Results

Behaviour of superalloy in rigid shell

Linear elastic model

If purely elastic properties are assumed for the metal, the thermal stress expected from cooling of a CMSX-4 bar under a rigid constraint can be estimated. Figure 4 shows the predicted strain evolution with temperature in this case, namely, the variation of thermal strain $\varepsilon^{\text{thermal}}$ and elastic strain $\varepsilon^{\text{elastic}}$ with temperature. The calculation is based upon a reference temperature of 1300°C, which is approximately the solidus temperature of CMSX-4.

One can see that the elastic strain increases monotonically with decreasing temperature in an approximately linear fashion. The thermal strain is of equal magnitude but opposite sign; thus, the sum of the two strains is zero

as assumed previously. The calculated stress is consistent with the strains given in Fig. 4 and increases approximately linearly with decreasing temperature; this is consistent with the FEM results for the VeriCAST blade, which are presented in Fig. 3. The calculated stresses, particularly below 600°C, are appreciably greater than the 0.1% proof strength (Fig. 4). This confirms that plasticity, both rate independent and at higher temperatures rate dependent, needs to be accounted for.

Elasto-plastic model

In the elasto-plastic model, the total strain is partitioned into elastic and plastic components. It can be seen in Fig. 5 that plastic deformation is predicted to occur from 1300 to ~1100°C, and then as the temperature falls further, the total accumulated plastic strain stays constant. Within this temperature interval, the behaviour remains elastic. When the temperature fall below ~650°C, there is a dramatic increase in plastic strain; at this stage, the elastic strain declines continuously. Clearly, the stress level predicted are very high, higher than the yield stress of the material at low temperatures, indicating that plastic yielding is a strong possibility. The stress results given in Fig. 6 illustrate the variation of calculated stress and yield stress with temperature. Above 1100°C, the predicted stress matches the experimental 0.1% proof strength, but at lower temperature, it falls below it. Below 650°C, thermal stress is again greater than the yield stress. Thus, in the absence of stress relieving mechanisms and certainly if stress concentration effects are present, plasticity must occur.

Elasto-visco-plastic model model

The elasto-visco-plastic model accounts for thermal, elastic, plastic and creep strains. Figure 7 summarises results from this model. Strains generated within the superalloy are illustrated in Fig. 8. It is clear that there are at least four zones in which differing behaviour is expected. In zone A, the superalloy starts yielding during the very early stages of the cooling process (between 1300 and 1200°C). This is because the proof strength is very low at these temperatures as shown in Fig. 8, and the thermal contraction stress exceeds it. In zone B, the proof stress increases rapidly to exceed the thermal stress; consequently, accumulation of plastic strain ceases. However, the temperature is still sufficiently high for creep strain to be accumulated from

1200 to 1000°C. Thus, creep and elastic deformation happens in this region. In zone C, from ~1000 to 600°C, the proof strength is above the thermal stress, so there is only elastic deformation in this zone. Finally, below 600°C in zone D, the proof strength is again much lower than the stress; as a result, plastic straining is predicted to occur and to continue up to 0.6%. The superalloy work hardens following the isotropic hardening criteria that has been assumed. During this stage, the stress build-up in the superalloy decreases but is slightly higher than the 0.1% proof strength, see Fig. 9. This region has a significant increase in plastic strain and a decrease in elastic strain.

The cooling rate used in the present work is 0.83°C s⁻¹, which is the same as VeriCAST model, the results from which are quoted in Fig. 1. The effect of the cooling rate during solidification is of interest. The effect of cooling rates of 0.1, 1 and 10°C s⁻¹ has been modelled as seen in Fig. 10. It can be seen that slow cooling rate can delay the significant increase in plastic strain within the superalloy.

Behaviour of superalloy in elastic shell and surrounding ceramic core

Effect of elastic shell

So far, the shell has been assumed to be perfectly rigid. Elastic deformation of the shell will now be taken into account. As before, it is assumed that the superalloy and shell adhere to each other during cooling.

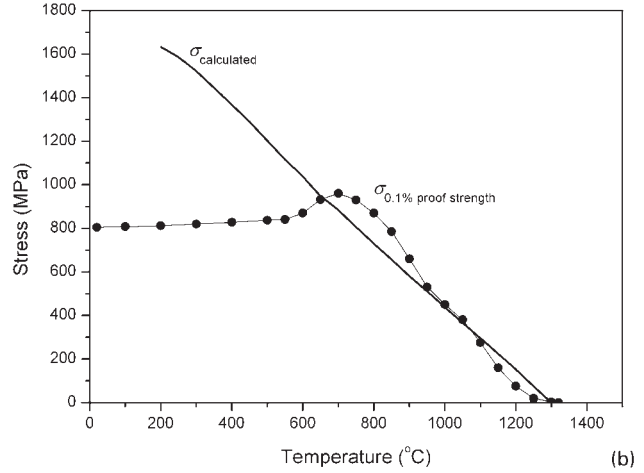
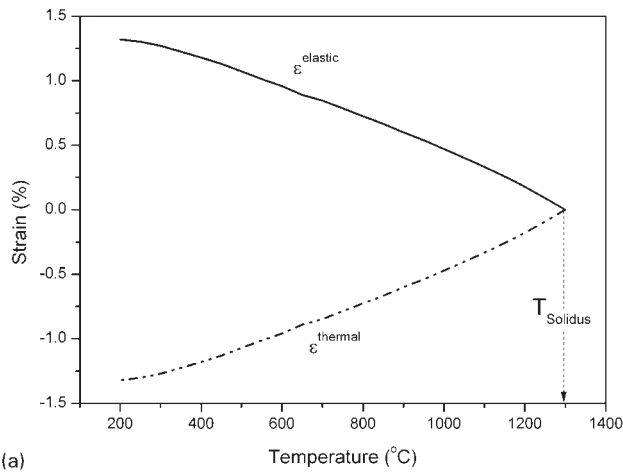
The results are shown in Fig. 11. One sees that the stress in the superalloy depends in a sensitive fashion upon the ratio $S_f^s = S_{\text{alloy}}/S_{\text{shell}}$ and therefore the thickness of the shell used. With a greater thickness of shell, the plasticity that is induced in the superalloy is larger. One can see that from Fig. 12 the plastic strain that built up within the superalloy, when taking elastic deformation of the shell into account, is lower than for

Table 1 Materials data for CMSX-4 used for analysis

Temperature/°C	CMSX-4			
	$E_{\text{alloy}}^{20}/\text{GPa}$	$\alpha_{\text{alloy}}^{21}/\times 10^{-6} \text{K}^{-1}$	σ_y^{22}/MPa	$\sigma_{\infty}^{23}/\text{MPa}$
20	127	6.0	805	935
100	125	11.4	808	943
200	122	12.0	812	958
300	118	12.4	820	970
400	114	12.7	828	993
500	110	13.0	838	1023
600	106	13.5	870	1064
700	101	13.9	960	1136
800	96	14.4	870	1195
900	90	14.9	660	1035
1000	84	15.6	450	757
1100	80	16.8	275	500
1200	75	18.5	75	173
1300	70	19.0	3	30

Table 2 Ceramic materials data used for analysis

Properties	Shells		
	Shell 1	Shell 2	Core
$E^{24,25}/\text{GPa}$	85	52	42
$\alpha^{26}/\times 10^{-6} \text{K}^{-1}$	8.2	5.1	10.4

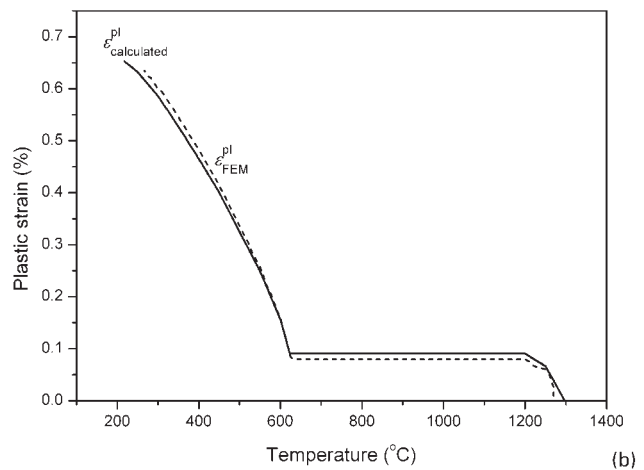
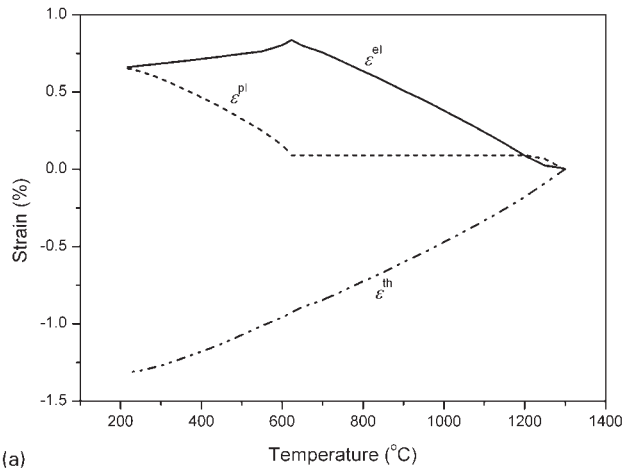


(a) strains built-up in uniaxial direction; (b) calculated stress
5 Stress and strain results from analytical method

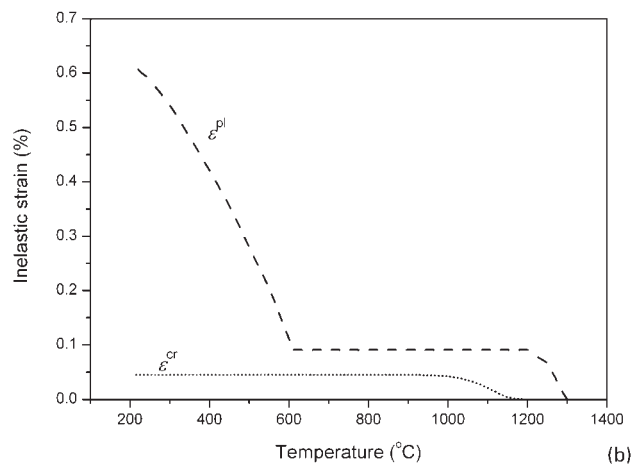
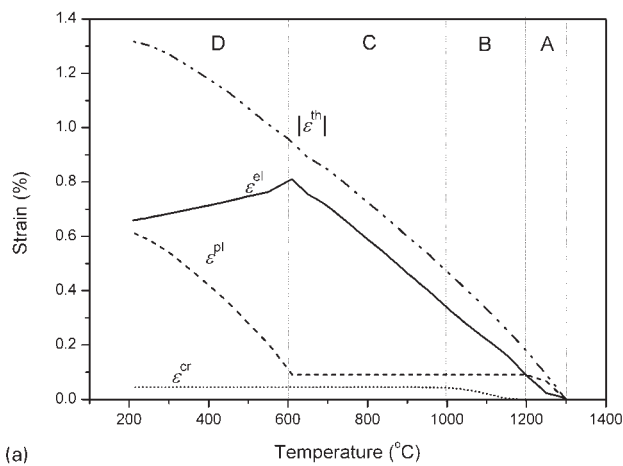
the superalloy individually. A magnification of Fig. 12 to reveal what is predicted at very low strain level is given in the top right of the figure. It is evident that very little plastic strain is induced when the superalloy cross-section

is larger than the shell. However, when the shell thickness is increased, the plastic strain is induced.

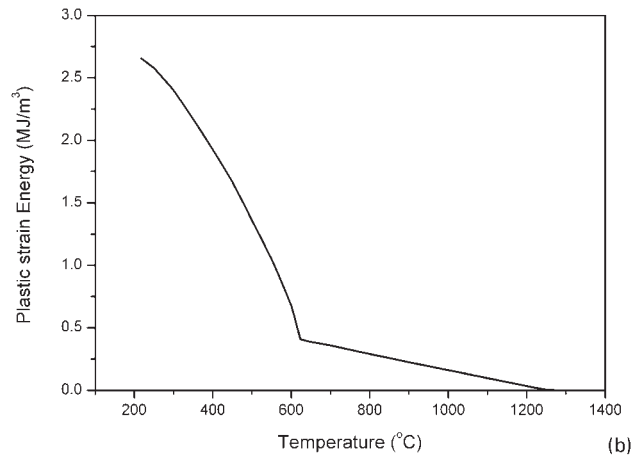
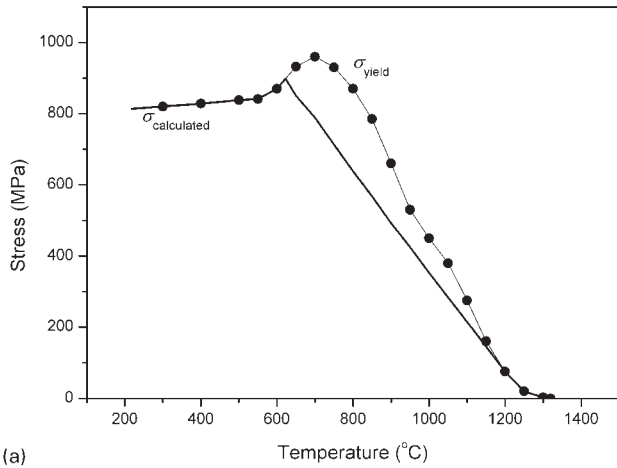
Because the plastic deformation is introduced at high temperature and its rate of accumulation decreases



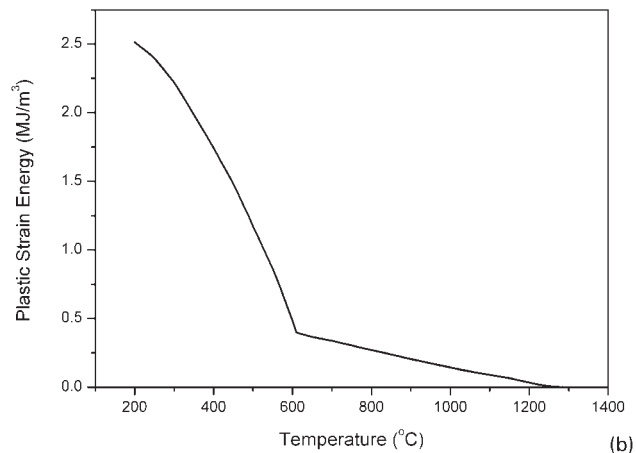
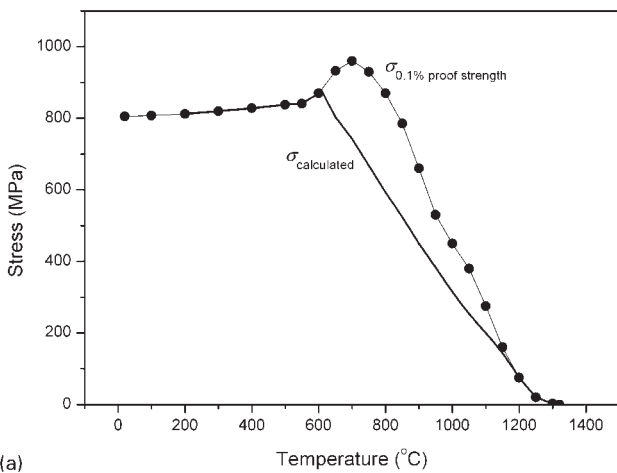
(a) strain diagram of elasto-plastic model; (b) predicted plastic strain from analysis and FEM
6 Calculated strains from elasto-plastic model



(a) strain diagram of elasto-visco-plastic model; (b) predicted inelastic strain
7 Strains evolution during casting calculated by elasto-visco-plastic model



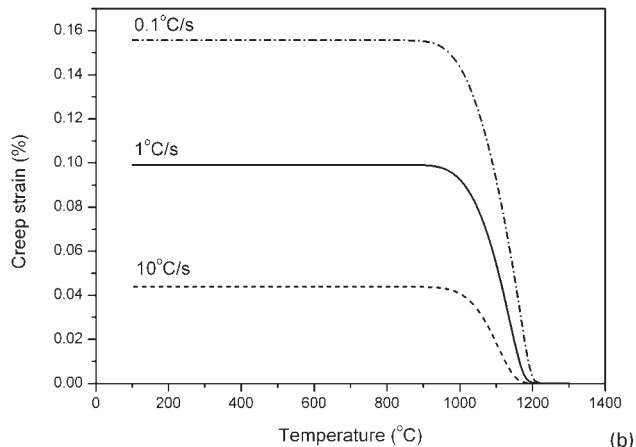
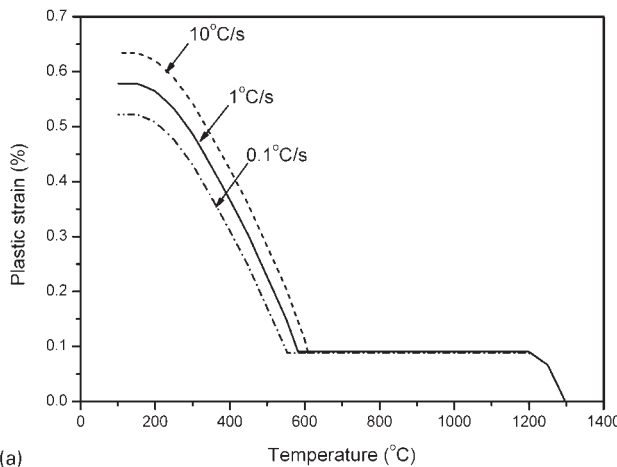
8 Calculated *a* stress and *b* plastic strain energy calculated from elasto-plastic model



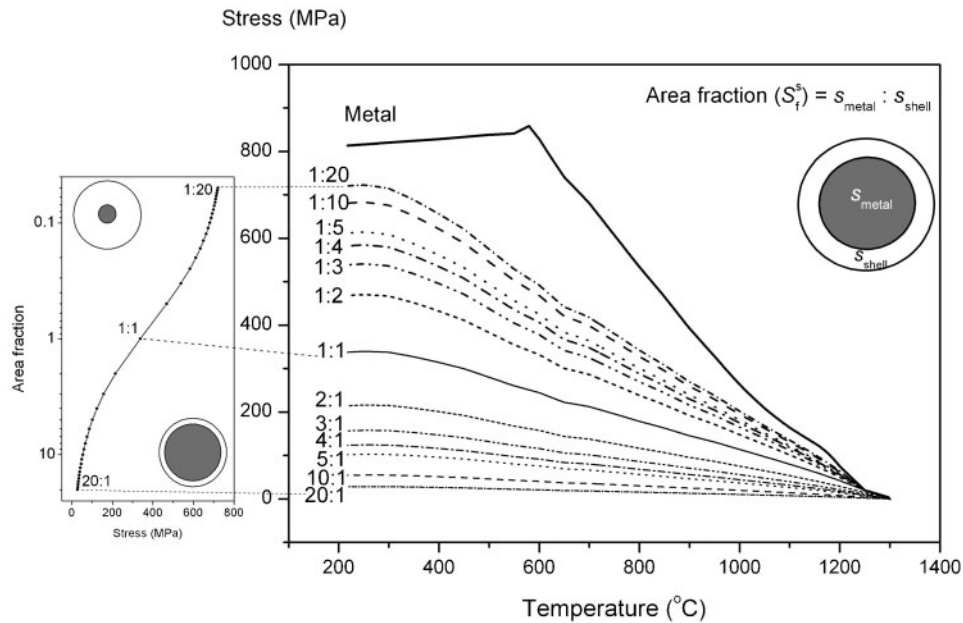
9 Variation of *a* stress and *b* strain energy with temperature simulated from elasto-visco-plastic model

markedly to a low level, one can summarise the results succinctly on a processing map (Figs. 12 and 13). The plastic strains quoted are determined at a final cooling temperature of 200°C. One can see that the accumulated plastic strain is rather low for an area fraction of

unity, but it increases quickly for smaller values as the ceramic shell thickens. Comparing the behaviour of the stiff and less stiff shells (shells 1 and 2, respectively), one finds that the stiffer shell promotes plastic strain in the metal and the less stiff shell allows a greater shell



10 Effect of cooling rates (0.1, 1 and 10°C s⁻¹) on *a* plastic strain and *b* creep strain simulated via elasto-visco-plastic model



11 Sensitivity of stress level within metal calculated by elasto-visco-plastic model to shell thickness

thickness to be used for a given permitted plastic strain level.

Effect of elastic ceramic core

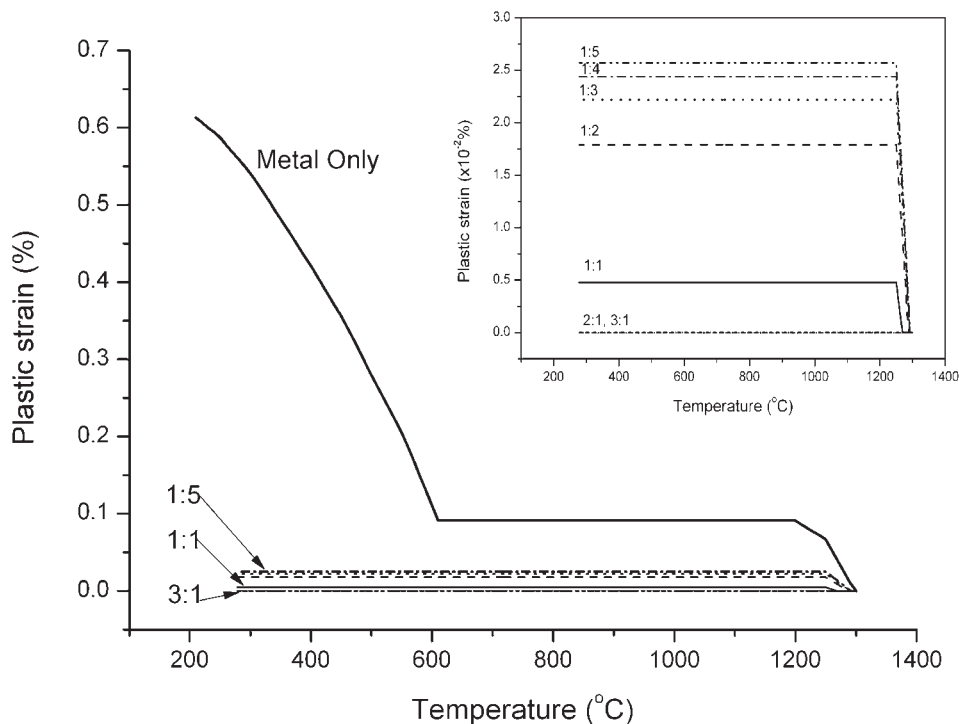
Cores for investment cast superalloys are usually silica based, and therefore, the shell 2 properties are appropriate for modelling its effect. It is assumed that the superalloy follows the elasto-visco-plastic model model.

The results given in Fig. 14 indicate that there is no plastic strain if the superalloy is larger than the core; on the contrary, if the core is larger than the superalloy, then the plastic strain becomes more substantial. The larger the ceramic core, the higher the strain within the superalloy. However, the predicted plastic strains are quite small, of the order 10^{-5} or 0.001%.

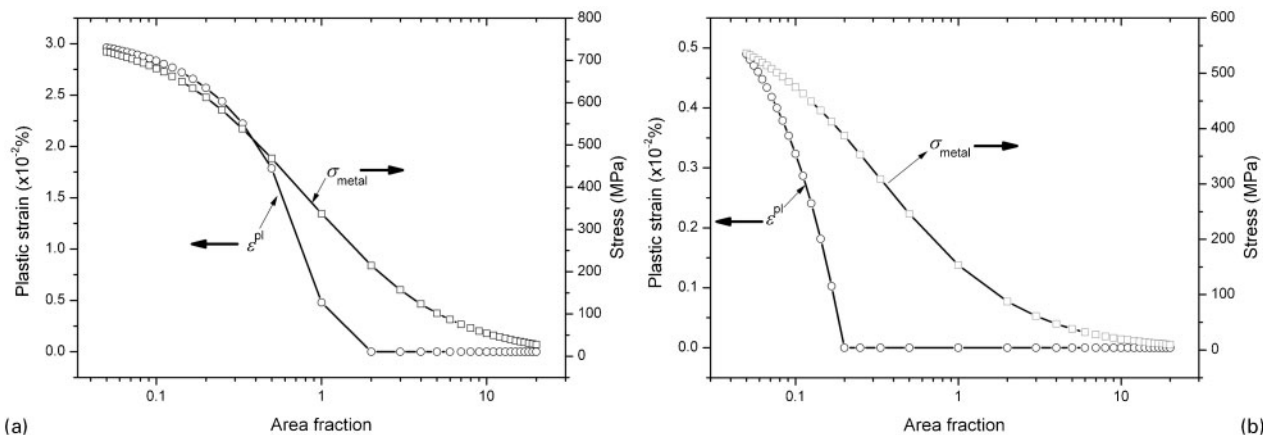
Stress relaxation

Figure 15 shows the stress relaxation behaviour when held at 1000, 1100 and 1200°C at different levels of applied stresses. Obviously, the stress relaxation is strongly depended on the creep mechanism within the superalloy. It can be seen from Fig. 15 that when we applied higher stresses at lower temperature and lower stress at higher temperature. Then, the stress is allowed to decline with time, and it seems to relieve faster at first place and slower later on for those three conditions: 400 MPa at 1000°C, 200 MPa at 1100°C and 50 MPa at 1200°C.

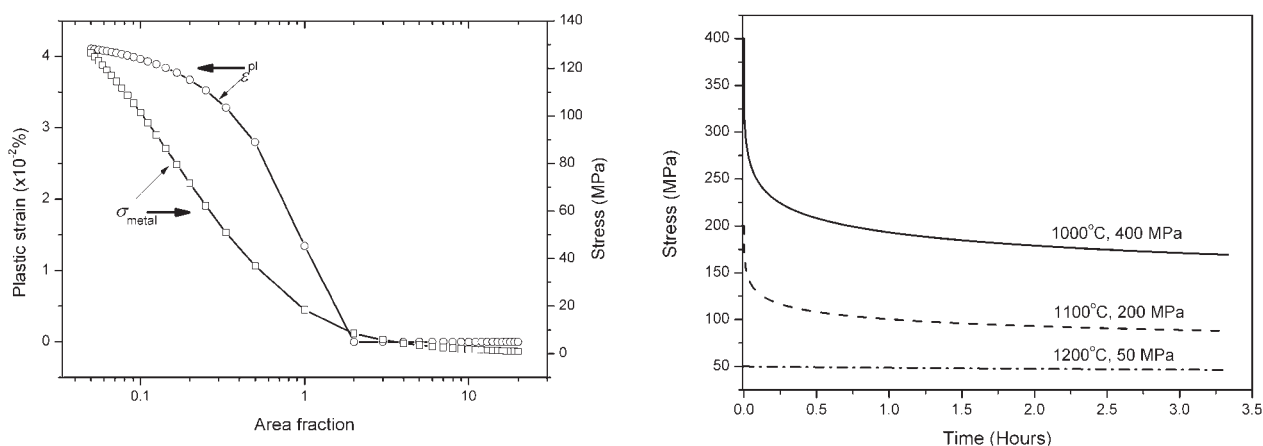
To clarify, time required for a half of applied stress is one of the indication of the effect during casting. However, ~3 h time is very relevant to solidification



12 Variation of predicted plastic strain within metal cast in different shell thicknesses



13 Variation of area fraction with stress and plastic strain at 200°C in a shell 1 and b shell 2 (stiffer shell)



14 Predicted plastic strain from couple of superalloy and core material

15 Stress relaxation behaviour at 1000, 1100 and 1200°C with applied stress of 400, 200 and 50 MPa, respectively

time during casting process. If this figure has been considered and we make use of the previous calculation results, it becomes clear that higher stress is expected to take place at lower temperature. To show this effect, relaxation behaviour has been simulated. Stress decreases very rapidly at 1000°C with 400 MPa applied stress. In the medium range of 1100°C with 200 MPa applied stress, the stress declines slower than 1000°C. Nevertheless, at 1200°C with 50 MPa applied stress, it is most likely that there is no significant change in stress within a few hours time. It shows obviously that temperature around 1000–1100°C is very pertinent to cause stress relief and consequently it might cause some cracks within the metal.

Conclusions

1. Finite element analysis of the investment casting of a single crystal superalloy into a typical turbine blade shape indicates that, for the aerofoil region, the thermal mechanical contraction can be approximated as 1D. Differential thermal contraction of shell and metal leads to tensile and compressive loading of metal and shell respectively.

2. One-dimensional semi-analytical models of a constrained bar of CMSX-4 have been made using three distinct constitutive models—linear elastic, elasto-plastic

and elasto-visco-plastic model models—with different shell and core conditions. For a perfectly rigid shell, plasticity is predicted to occur in two regimes: between 1150 and 1000°C by creep time dependent deformation and by time independent tensile straining below 650°C.

3. Assuming a shell system that remains elastic, the plastic strain induced in the metal casting has been predicted for the 1D situation. It is demonstrated that the plastic strains induced can be significant. With increasing shell thickness, the stress within the superalloy is increased. Stiffer shells lead to greater strains in the casting.

4. Shrinkage around a nominally elastic ceramic core has been studied. This situation is analogous to the strain induced on the inner surface of a turbine blade. The sensitivity of the plastic strain induced to the thickness of the ceramic core has been rationalised.

5. In general, the modelling reveals the importance of correctly accounting for the high temperature deformation; plastic deformation initiates at high temperature above 1100°C.

6. The 1D models provide the basis for further development of two- and three-dimensional analysis, which will be more representative of the true geometrical features that are present in a typical turbine blade casting. The presence of stress concentration features and perhaps shell fracture during cooling are worthy of further consideration.

Acknowledgements

The primary author (CP) thanks the Engineering and Physical Sciences Research Council of the UK and Rolls-Royce plc for a Dorothy Hodgkin Postgraduate Award.

References

1. P. R. Rios, F. Siciliano, Jr, H. R. Z. Sandim, R. L. Plaut and A. F. Padiha: *Mater. Res.*, 2005, **8**, 225–238.
2. R. D. Doherty, D. A. Hughes, F. J. Humphreys, J. J. Jonas, D. J. Jensen, M. E. Kassner, W. E. King, T. R. McNelley, H. J. McQueen and A. D. Rollett: *Mater. Sci. Eng. A*, 1997, **A238**, 219–274.
3. H. T. Pang, L. Zhang, R. A. Hobbs, H. J. Stone and C. M. F. Rae: *Metall. Mater. Trans. A*, 2012, **43A**, (9), 3264–3282.
4. N. Warnken, H. Larson and R. C. Reed: *Mater. Sci. Technol.*, 2009, **25**, 179–185.
5. A. J. Fletcher: 'Thermal stress and strain generation in heat treatment'; 1989, Essex, Elsevier Science Publishers Ltd.
6. K. Heck, R. Blackford and R. F. Singer: *Mater. Sci. Technol.*, 1999, **15**, 213–220.
7. A. R. Mashreghi, H. Monajatizadeh, M. Jahazi and S. Yue: *Mater. Sci. Technol.*, 2004, **20**, (2), 161–166.
8. D. C. Cox, B. Roebuck, C. M. F. Rae and R. C. Reed: *Mater. Sci. Technol.*, 2003, **19**, 440–446.
9. W. Tu and T. M. Pollock: *Metall. Mater. Trans. A*, 2010, **41A**, (8), 2002–2009.
10. C. L. Brundidge, D. van Drasek, B. Wang and T. M. Pollock: *Metall. Mater. Trans. A*, 2012, **43A**, (2), 965–976.
11. J. Safari, S. Nategh and M. McLean: *Mater. Sci. Technol.*, 2006, **22**, 888–898.
12. V. Choi, T. Parthasarathy, D. Dimiduk and M. Uchic: *Metall. Mater. Trans. A*, 2006, **37A**, 545–550.
13. P. Carter, D. C. Cox, C. A. Gandin and R. C. Reed: *Mater. Sci. Eng. A*, 2000, **A280**, 233–246.
14. K. Saï, V. Aubourg, G. Caillietaud and J. L. Strudel: *Mater. Sci. Technol.*, 2004, **20**, 747–755.
15. C. Panwisawas, H. Mathur, J.-C. Gebelin, D. Putman, C. M. F. Rae and R. C. Reed: *Acta Mater.*, 2013, **61**, (1), 51–66.
16. H. J. Dai, J.-C. Gebelin, M. Newell, R. C. Reed, N. D'Souza, P. D. Brown and H. B. Dong: Proc. Superalloys 2008 Conf., Seven Springs, PA, USA, September 2008, The Metals Society, 367–374.
17. M. Newell: 'Aspects of a novel casting process for the production of nickel-based superalloy high pressure turbine blades', PhD thesis, The University of Birmingham, Birmingham, UK, 2009.
18. K. F. Riley, M. P. Hobson and S. J. Bence: 'Mathematical methods for physics and engineering', 2nd edn; 2003, Cambridge, Cambridge University Press.
19. D. A. Woodford: *JSME Int. J.*, 2002, **45**, (1), 98–103.
20. D. Siebörger, H. Knake and U. Glatzel: *Mater. Sci. Eng. A*, 2001, **A298**, 26–33.
21. P. N. Quested, R. F. Brooks, L. Chapman, R. Morrell, Y. Youssel and K. C. Mills: *Mater. Sci. Technol.*, 2009, **25**, 154–162.
22. R. C. Reed: 'The superalloys: fundamentals and applications'; 2006, Cambridge, Cambridge University Press.
23. D. W. MacLachlan and D. M. Knowles: *Mater. Sci. Eng. A*, 2001, **A302**, 275–285.
24. S. V. Nair and K. Jakus: 'High temperature mechanical behavior of ceramic composites'; 1995, Boston, Butterworth-Heinemann.
25. W. Pabst, E. Gregorová, G. Tichá and E. Týnová: *Ceramics-Silikáty*, 2004, **48**, (4), 165–174.
26. D. J. Green: 'An introduction to the mechanical properties of ceramics'; 1998, Cambridge, Cambridge University Press.